UNIVERSITAT POLITÈCNICA DE CATALUNYA

UNIVERSITY OF CALIFORNIA, SAN DIEGO

Bachelor's Thesis in Engineering Physics

Carbon-Coated TiO_2 Nanoparticles as advanced anode material for Lithium-Ion Batteries

Alba Martínez

Supervisors:

Prof. Zheng Chen
Prof. Jordi Llorca Piqué

Barcelona
October 2017

Abstract

Engineering Physics

Carbon-Coated TiO_2 Nanoparticles as advanced anode material for Lithium-Ion Batteries

By Alba Martínez

Lithium-Ion Batteries (LIBs) are no stranger to the everyday-portable-electronics users. Their high energy density and cycle life place these devices to the must-have list of an extensive selection of applications. Having to provide coverage to so many different fields of study, the requirements in each of them are very likely to differ.

For this reason, the future energy storage and power improvement of LIBs is of great interest and it never ceases to seek new techniques to further enhance the components' properties. Focusing on the battery's electrode and, more precisely, the anode material, will be an effective approach to achieve this goal.

To date, very intensive research on anode materials has been done, with special focus on carbon-based nanostructured materials to focus on surface area and conductivity improvement, for further implementation of LIBs in higher-rate performance systems. Furthermore, the environmental impact of these devices has become a crucial matter to take into account when investigating on the field. So environmentally-friendliness along with low production costs have become key features the future devices must include.

This project presents an approach to synthesize nanostructured crystallites using a very simple, versatile and cheap two-phase hydrothermal method for tunable particle properties. Anatase TiO_2 nanoparticles have been synthesized as anode material, for its abundance, great structural stability, low volume change, non-toxicity and safety. Despite its poor conductivity, it has been fixed with a carbon coating of the TiO_2 nanoparticles under N_2 annealing at temperatures of 500, 600 and 700°C. Coating effects and size effects have been tested with an air-sintered carbon-free TiO_2 and a commercial TiO_2 (P25) control samples, respectively. XRD, TEM and BET characterization techniques confirm the obtaining of mesoporous carbon-coated anatase TiO_2 nanospheres of estimated 4 nm in size covered in a single carbon layer. Coin cells have been assembled using the as-prepared materials and an electrochemical analysis of the galvanostatic charge/discharge curves and the EIS have been conducted, showing a better performance of TiO_2@C-500 over the other materials. Improved capacity, coulombic efficiency and capacity retention for long cycle life battery performance.

Acknowledgements

I would like to express my sincere gratitude to Prof. Zheng Chen for his mentorship and accepting me as a member of his research team with little prior knowledge of my experience nor my background. I am deeply grateful for having been entrusted this project and for him having left the doors open for me to have the chance to participate in future projects in this field.

I would also like to express my thankfulness to my laboratory colleagues for such a warm welcome to the team, and more concretely to Yang Shi and Fei Ji for having lent me their time to teach me and help me regardless of their busy schedules. Their great effort, hard work and passion put into their research motivated me to carry my project forward.

I cannot forget to thank the teachers that have walked this journey as an Engineering Physics student with me. Their expertise and passion aren't anything else but an inspiration at its purest. I would like to specially address my gratitude to Jordi Llorca for introducing me to this amazing world that is nanoscience and nanotechnology. Not only because it is indeed a fascinating world, but more importantly because his genuine enthusiasm towards his job and research got to me at the right time.

I am extremely thankful for my friends in UC San Diego, who have this experience an unforgettable one. Also, my biggest thank you to my friends back home who never fail to make me feel like I never left, and to my UPC friends, for sharing this incredible journey with me and upgrading this amazing experience that is university.

Last, but by no means least, I could not be thankful enough to my family, who is the main reason behind any little success, whether it be academic or personal. Their unceasing support and love are the little engine that has pushed me to achieve my goals.

Contents

Chapter 1

Introduction

It is no surprise that Lithium batteries are a matter of importance and great popularity in the technologic world today. Portable electronics, implantable devices, renewable energies, hybrid/full electric vehicles (EVs), and a broader range of fields within the energy storage framework are giving Lithium batteries a great relevance and interest. In this chapter, a brief introduction to LIBs and its highlights is presented along with the goals to achieve with this project.

Batteries being very promising high-performance energy-storage devices has taken research towards testing new electrode materials to improve energy and power densities for better performance. However, environmental protection, low manufacturing cost and safety have become the main features needed in all modern battery technology. Such priorities have led to the rejection of unsafe, toxic, hazardous materials that were being used in the preceding battery systems (e.g. metal lithium based battery anodes[1]).

Lithium is the lightest of all metals, showing a large electrochemical potential and high energy density relative to its weight. Lithium metal has been consistently studied in an attempt for it to be the "it" material for lithium batteries, but it failed due to safety issues. However, it was found that the usage of lithium ions instead was a lot safer. LIBs are chemically less reactive, safer, and offer longer cycle life than metallic lithium batteries. Hence, the study of lithium ion, lithium sulfur, and lithium air batteries has emerged due to not only their reduced size (Li-ion), lightness (Li-S), or the combination of both (Li-air), but also their undeniable improved structures using lower cost, safer materials[2].

Nonetheless, more extensive research needs to be done to overcome some existing challenges that are hampering the proper development and improvement of Li-ion batteries. The battery market is ambitious and does not cease to adapt their devices to our society's fast-paced lifestyle. For that reason, the same properties that make LIBs stand out from other technologies need to be continuously enhanced: minimizing manufacturing costs, boosting mass production, and synthesizing more environmentally-friendly recyclable materials.

It is undeniably the main research focus have been anode materials and the different approaches to obtain improved electrochemical properties as well as lower manufacturing costs and simpler techniques. These characteristics flash a light on TiO_2 as a good and promising candidate. Amongst the advantages of TiO2 as a promising material in anodes, it shows fast lithium ion diffusion; it's low cost; environmentally friendly; guarantees good safety, since it is a benign material; its anatase phase is very stable, so a low SEI forms leading to a longer life material in the Li-ion cell, also it only presents <4% of volume change after cycling; reversible capacity. For these many reasons, TiO2 is a good candidate for current research on Li-ion batteries and future application. Nonetheless, very little work has been done up to date, which leaves a knowledge gap when referring to this material. Some issues have yet to be improved, such as its slow capacity; low electrical conductivity; poor rate capability for higher density current battery cycling.

Aims of this project

The main objectives of this work are: (1) to find a versatile, simple, low cost mechanism to synthesize size-tunable and shape-controlled TiO_2 5 nm nanoparticles and to use an effective method to produce core-shell carbon-coated TiO_2 at the most suitable annealing temperature to avoid nanoscale aggregation and to obtain enhanced particle surface area and conductivity. (2) To assemble these materials into an electrode and further battery coin cell for further electrochemical characterization to analyze its cycling performance.

Chapter 2

State Of The Art & Theoretical Background

A brief introduction to the motivation leading this research has been presented. A deeper contextualization giving some theoretical facts is then needed to further understand the chemistry and processes behind the main topics in this report. Therefore, in depth concepts regarding Lithium Batteries and its different approaches to different applications are firstly presented, being Li-Ion batteries the main focus. Afterwards, a breakdown of these devices materials is carried out and information about materials of interest to date is given away.

2.1 Li-ion Batteries

In recent years, Li-ion batteries' presence in high-energy performance technologies has grown very strongly. In the context of the battery industry aiming to obtain greater specific levels of performance for a wider range of applications at lower costs, intensive research work has been devoted towards the understanding and development of these devices. That's the reason of current research having been left with a very valuable heritage for the so called rechargeable batteries[3].

Having such good energy density for charge storage, Lithium happens to be the most appealing out of all metals when it comes to battery elaboration. What's more, LIBs outperform most of their fellow technologic devices with higher specific capacities (around 150mAg^{-1}), energy density (~200-400 WhL^{-1}), longer cycle life (≥1000 cycles), and broader temperature operating range (-20°C to 65°C), to quickly mention a few[4].

But what is a lithium ion battery?

2.1.1 Common Li-ion Battery Structure

Even though thorough research and several variations of the lithium ion cell structure has been carried out to improve its properties, an introduction to the common components composing it is presented.

A simple structure of three components conform the design of a Li-ion battery. Two electrodes made out of different active material give each of them a different chemical nature: the negative electrode – or anode –, and the positive electrode – or cathode. The separator is the third component, and it is located between the two electrodes, providing with both electronic insulation so no short circuit occurs, and ionic conduction, so a proper diffusion of the Li ions is guaranteed during the charging and the reverse discharging process. The three-element system is soaked in a liquid solution, the electrolyte – consisting of Li salt (i.e., $LiPF_6$) dissolved into an alkyl organic carbonate –, which provides the Li ions with channels to travel through the separator from one electrode to the other.

The material used in the **anode** is typically graphitic carbon. Graphite, the most used one, improves insertion of the Li ions being able to store them through the interstitial sites between to graphite planes (Fig.2.1). Being a cheap, durable material showing low expansion, great porosity, cycle efficiency and a moderate capacity (372 mAhg^{-1}), graphite has been the go-to material for the anode this past decades[5].

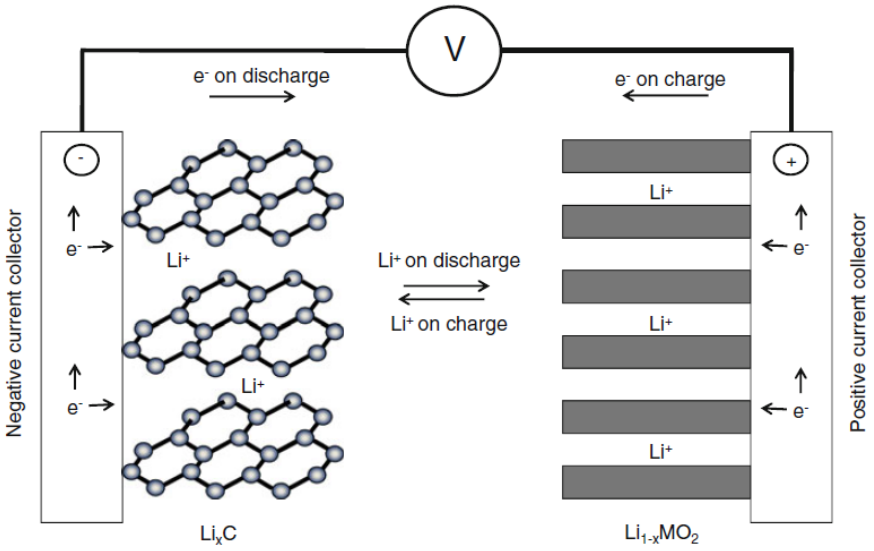

Figure 2.1. Representation of the discharge and charge processes taking place in a LIB.

In the case of the **cathode**, the most frequently used materials, and the most promising ones, are from the $LiMPO_4$ family – where M is a transition metal[6]. Cathodes using different amounts of three transition metals $Li(Ni,Mn,Co)O_2$ is showing the present research high capacities, good rate capabilities and high operating voltages[7].

In both cases, the electrode consists of a metal foil coated with the respective active materials – copper foil for the anode, and aluminum foil for the cathode –, mixed with a high-surface-area carbon black as an electronic enhancer, and polyvinylidene fluoride (PVdF), a fluorinated polymer acting as a binder. The reactions taking place in each electrode are shown in Fig.2.2.

Positive electrode

$$LiMO_2 \underset{\text{discharge}}{\overset{\text{charge}}{\rightleftharpoons}} Li_{1-x}MO_2 + xLi^+ + xe^-$$

Negative electrode

$$C + xLi^+ + xe^- \underset{\text{discharge}}{\overset{\text{charge}}{\rightleftharpoons}} Li_xC$$

Overall cell

$$LiMO_2 + C \underset{\text{discharge}}{\overset{\text{charge}}{\rightleftharpoons}} Li_xC + Li_{1-x}MO_2$$

Figure 2.2. Reactions occurring in the positive electrode and the negative electrode when charging and discharging.

As for the **separator**, having the role of allowing the transfer of the lithium ions between both electrodes, good permeability, porosity, as well as chemical, mechanical and thermal stability are needed requirements for the composing material. Such material is often a polymer matrix, mostly formed by poly(vinylidene fluoride), PVDF, or copolymers, since they show high polarity and dielectric constant for a good ionization of the lithium salts.

2.1.2 Technology Behind Lithium-ion Cells

In order to investigate which next generation materials LIBs should improve in and further investigate in, a brief framework is needed regarding their basic chemistry.

Lithium-ion batteries are given that name due to the usage of lithium intercalation compounds as the positive and negative electrode materials within its comprised cell structure (Fig.2.3). The typical mechanism taking place inside the cell is called "rocking chair, since a transport of lithium ions is moving back and forth due to the extraction and insertion at the electrodes[8].

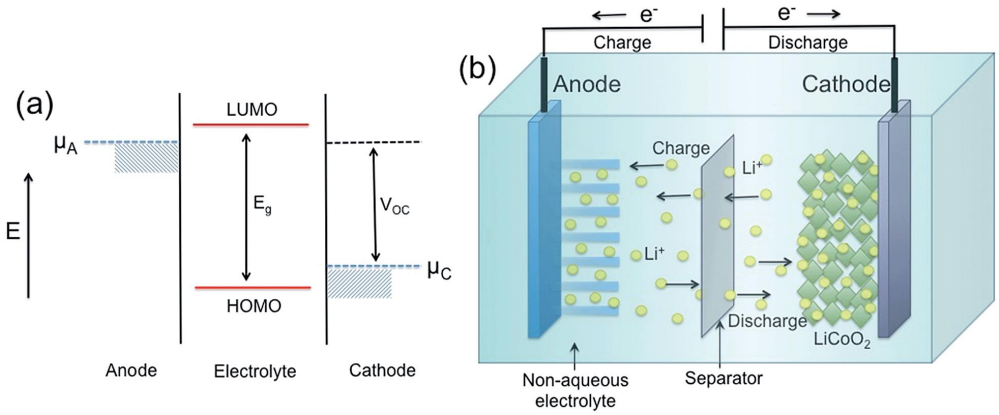

Figure 2.3. Energy levels of the anode and the cathode compared to the charge/discharge processes inside the cell.

During **charge** of a battery, the cathode is oxidized and the lithium ions are de-intercalated or extracted due to the applied electrochemical force. These travel to the anode, which is going to be reduced when the Li ions are intercalated in the matrix. This process is projected simultaneously in the external circuit, since every electron related to its respective extracted Li ion leaves the cathode and is accepted by the anode to balance the reaction inside the cell.

When in **discharge**, the reverse procedure takes place: electrons travel through the external circuit while Li ions are de-intercalated from the anode and accepted by the cathode. That powers up any connected system during the process from the conversion of chemical energy into electrical energy.

Therefore, the basic concept to remember is charging of a battery implies electrons moving from the cathode to the anode; whereas discharging means electrons are moving from the anode back to the cathode.

2.2 State-of-the-Art Anode Materials for LIBs

The rocking chair process occurring inside the cell is a highly reversible reaction which consecutives extractions and insertions may cause the material to suffer from volume change of the electrodes. Thus, finding a material which nature will avoid the matrix degradation over time due to that change in volume is of great interest.

For that matter, current research in LIBs has recently been focused on the development of electrode materials. In fact, within recent years a great variety of cathode materials have been developed. However, there's still an urgency to replace anode materials to tackle the low power density problems of graphite[9]. Taking such step would broaden the spectrum of new applications for these high-energy storage devices.

Starting off from the base materials composing Li-ion batteries, the performance of these devices cannot be further improved if these remain unchanged. Such continuity with the use of Lithium-carbon-based materials for the negative electrode is funded in the premises of carbon-based materials having a good electrochemical behavior; being a low cost option; and having a structure that provides good intercalation chemistry and good reactivity towards lithium.

State of the art of anode materials for LIBs are commonly classified depending on their Li-ion reaction mechanism. For the sake of simplicity, the three main groups are presented: alloy, conversion and intercalation materials[10]. In each of the cases there are a series of advantages as well as disadvantages, which may or may not be resolvable. An advanced material that can balance out those issues is the main goal of high-energy storage research.

Alloy materials (such as Si, Ge, Sn, Al, Bi, SnO2, etc.), for instance, even though they present the highest specific capacities amongst the materials in the other groups, large irreversible capacities as well as great capacity fading makes these alloy materials not so appealing for daily use Li-ion batteries.

Conversion materials – like transition metal oxides (Mn_xO_y, NiO, Fe_xO_y, Cu_2O, MoO_2, etc.), metal sulphides, phosphides and nitrides (M_xX_y, with X = S, P, N) –, showing high specific capacity and energy, as well as being low cost material and environmentally friendly, they yet lack good cycle life, more stability for SEI formation[11], or lower production costs.

Insertion materials – such as carbon based materials, carbon nanotubes, graphene, TiO_2, etc. – often have very low theoretical capacities, however they have shown the best capacity retention. Within this group, titanium based oxides present better properties than carbonaceous materials. Having very reversible reactions, very low volume change, safe materials as well as abundant and low-cost production, Titania (TiO_2) – shows higher theoretical capacity within the family group –, is a very promising anode material suitable for the next generation LIB materials[12].

2.2.1 TiO_2 as anode material

Some work has been done to study the chemistry of TiO_2 and its suitability as a promising anode material and, thus, good for lithium intercalation. But before diving into the benefits of using this material in Li-ion batteries, a basic introduction to TiO_2 is given.

TiO_2, or Titania, is one of the most recurring transition metal oxides (TMO) for high-energy storage technologies. It's an important wide-bandgap semiconductor (Eg around 3eV), which gives its poor electrical conductivity (10^{-12} – 10^{-7} $s{\cdot}cm^{-1}$)[13]. According to the reaction below (1), the reversible Li ion insertion and extraction from TiO_2 occurs:

$$xLi^+ + xe^- + TiO_2 \rightarrow Li_xTiO_2 \qquad (2.1)$$

TiO_2 can host 1 mol of lithium per 1 mol of TiO_2 showing a theoretical maximum capacity of 330 $mAhg^{-1}$. Therefore, x can range between 0 and 1. Achieving such capacity and a certain x value depends strongly on the TiO_2 structural parameters such as the polymorphs, particle size, surface area and crystallinity. Titania is commonly presented in these four well-known different structures: rutile, brookite, anatase, and TiO_2 (B). The two former phases, rutile and brookite, are the more densely stacked structures, thus showing a very poor lithium insertion due to preferred Li^+ sites being already occupied. The two latter phases, anatase and TiO_2 (B), are the less dense among the four, and present a promising structure for good lithiation in the cell.

Rutile, despite being the most stable structure for TiO_2, its nature and stacking makes the cations preferred site to be that of oxygen octahedral vacancy[14][15]. Li ions occupying the voids induces a series of mitigations within the lattice (Fig.2.4(a)), which turns into a highly anisotropic Li^+ diffusion resulting in volume change. Such alteration would end up damaging the material and, thus, shortening the battery's lifecycle.

Alongside with rutile, **brookite** phase (Fig.2.4(b)), being the second densest structure among the four, shows a very poor lithium insertion and extraction leading to unwanted relocations within the matrix and, thus, worse capacity and performance.

Anatase is found to be the most stable when it comes to lithium intercalation due to the stacking of 1D zigzag chains, which leaves gaps within the anatase framework (Fig.2.4(c))[16], where great insertion of the Li ions leads to minimum volume change (3 – 4% of the unit cell volume)[17]. Thus providing the battery with a longer cycle life.

TiO_2 (B) (Fig.2.4(d)) together with anatase are the most promising structures for LIB technology. It being the less compact TiO_2 structure, the lithium ions inserted in the matrix are expected to be very mobile and the bulk to have a greater capacity contributing to lithiation[18] [19]. Nevertheless, even having very good properties, TiO2 (B) structure fails at the initial charge-discharge cycle showing a significant irreversible capacity loss[20].

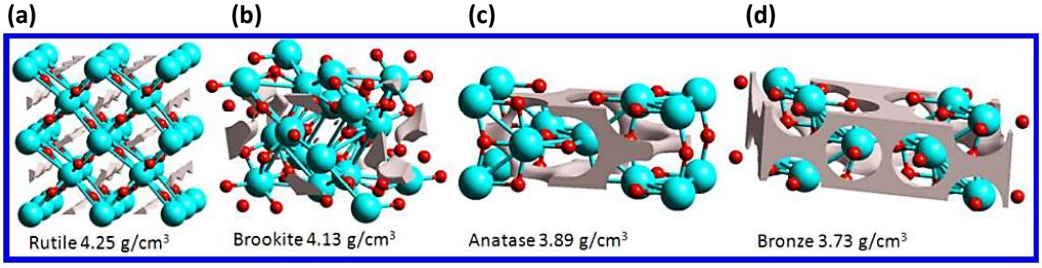

Figure 2.4. Structure representation of the titania rutile, brookite, anatase and (B) phases with the preferred Li ions intercalation sites (red dots).

Anatase has a tetragonal structure with the Ti^{4+} ions at the 4a octahedral sites and the O^{2-} ions at the 8e sites. The preferred site for the insertion of the Lithium ions during discharge are the empty 4b octahedral sites, like depicted in Figure 2.5.[21]

A full filling of all the empty channels in the anatase framework leads to a stoichiometry of $LiTiO_2$, where x from equation (2.1) is equal to the maximum value 1. Such value is unlikely to happen. However, anatase being the most studied TiO_2 phase due to its interesting properties, it has been reported to have a capacity of about $x \sim 0.6$ Li ion in Li_xTiO_2 at 1.78V *vs.* Li^+/Li^0. Despite not having the highest of capacities, its structure, interaction with the Li ions and stability, spikes anatase's reliability.

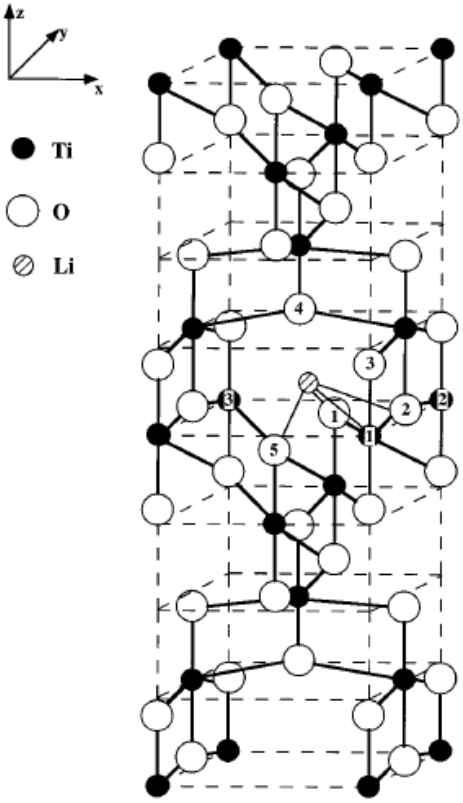

Figure 2.5. Equilibrium position of the inserted Li atom in the anatase bulk voids.

2.2.2 Carbon Coated TiO_2 Nanostructured Particles

Different procedures can be approached to overcome anatase TiO_2's deficiencies, taking into account the high dependency on its structural parameters to show specific electrochemical performance.

One of the biggest drawbacks is TiO_2 low capacity. Working in the nanoscale, it is known that nanostructuring results in higher surface area of the material, the smaller the particle the greater the surface to volume ratio. Having that in mind, an increased surface area means the material has a higher porosity, that is, the electrolyte has more open channels for it to penetrate the material, thus increasing the electrode-electrolyte contact area[22]. A greater surface area will also form more active sites for Li ion transport. Lithium ions will occupy the vacancies at the surface, rather than those in the bulk material, shortening the diffusion path length and time of the conducting species. Thereby, higher rate performance or density current will be achievable by the Li-ion battery.

Nevertheless, nanostructuring and working in such little scales usually results in nanoparticle agglomeration which, if severe, may defeat the purpose of the procedure. This problem can be prevented by coating or combining the nanoparticles with a second phase material that will improve the main material's porosity as well.

Carbon coating has been broadly studied to be a good approach to increase TiO_2 surface area, providing the material with more active sites on the surface. Moreover, it can enhance electron transport and avoid aggregation acting as a passivation layer of active materials. In addition to using TiO2 for being a safe material, carbon coated materials show a thinner SEI (solid electrolyte interphase), increasing the initial charge-discharge efficiency.

Combining nanostructuring of the TiO2 with the nanoparticles coating in carbon, will enhance the diffusion kinetics in the Li-ion cell with improved anode material.

Chapter 3

Experimental Method

In previous chapters, a brief introduction to the high-energy storage new technologies has been presented alongside with some theoretical framework to help understand the parties implied in the process of Lithium ion battery production. Following up this introductory framework, in this segment it is aimed to give an accurate explanation of the procedures carried out to obtain the desired nanostructures and the final product battery.

3.1 Carbon-Coated TiO_2 Nanoparticles Synthesis

Carbon-coated TiO_2 nanostructured particles have been synthesized in two different stages. The first stage consists on the synthesis of the TiO_2 nanoparticles via a two-phase hydrothermal technique. The second stage proceeds with the coating of the previously synthesized NPs with carbon under N_2 atmosphere at 500, 600 and 700°C for a proper study of the temperature effects on the coating and the overall TiO_2 annealed structure[23]. Furthermore, a 450°C annealed sample under air atmosphere has been prepared to compare the coating/non-coating electrochemical effects as anode material.

3.1.1 Synthesis of TiO_2 Nanoparticles

A two-phase hydrothermal route has been used to synthesize high-quality anatase TiO_2 nanoparticles. This is a simple, inexpensive, high-yield mechanism that facilitates the production of nanocrystals with customizable size, shape and dispersibility of the final product by adjusting the reaction parameters (concentration of the surfactant, reaction duration or the temperature)[24] [25]. Such control over the reaction products is what gives access to easily tunable TiO_2 properties and ways to improve its deficiencies.

The same two-phase procedure has been undergone by all the samples reported. In a typical synthesis, the water phase (A) consisted of 0.4 mL of *tert*-butylamine dissolved in 40 mL of DI water. The solution was transferred to a 100 mL Teflon-lined stainless-steel autoclave. Subsequently, the organic phase (B), with 0.6 g of Ti(IV) *n*-propoxide (TTIP) (2 mmol) and 4.0 mL of oleic acid ($C_{18}H_{35}COOH$, OA) was dissolved in 40 mL of toluene, and then transferred carefully with a pipette to the autoclave with A at the bottom, avoiding any stirring. It is crucial that there's no mixing of A with B, since the reaction takes place at the interphase, where the final product is going to form and dissolve in the organic phase[26]. These steps were followed under room temperature air conditions.

The autoclave was sealed and transferred to an oven at 180°C for 8 h, and later cooled down to room temperature. The organic phase was removed and saved, with special caution when piping it out close to the interface, since no TiO_2 nanoparticles remain in the aqueous phase. The water was discarded and the oil phase proceeded to have the nanoparticles removed. To do so, the TiO_2 nanoparticles were precipitated with methanol (20% - 30% of the volume) and later isolated by centrifugation at 2600 rpm for 2 min.

Further decantation of the supernatant was done, the precipitate was washed with 20 mL of toluene until dissolved and a second precipitation of the active material was done by adding that 20 – 30% of methanol (35 to 40 mL of TiO_2 needed around 10 to 12.5 mL of methanol). That was centrifuged under the same conditions and the final TiO_2 nanoparticles were left to air dry completely under the fume hood.

Having used surfactant molecules in this two-phase technique is very convenient to prevent agglomeration of the nanoparticles, since the resulting TiO_2 nanocrystals comprise an inorganic core capped with the carboxylic groups of OA. This will create a barrier providing electronic and chemical passivation of the surface and, thus, avoid any uncontrolled growth. Moreover, having this organic capping on the outer layer can be used for further particle manipulation, such as a precursor for a carbon layer formation[27].

3.1.2 Carbon-Coating/Uncoating of TiO_2 Nanoparticles

The dried TiO_2 NPs were manually grinded using a mortar. The powder was then transferred into a crucible and carbonized in a tubular furnace at 500, 600 or 700°C under N_2 atmosphere. In each case, the samples under N_2 flow at room temperature for 30 minutes and further heated to the respective 500, 600 or 700°C at 5°C/min, held at that temperature for 3 h and slowly cooled down back to room temperature.

Another synthesized TiO_2 NP batch was used as a control sample for coating effect comparison. The material was transferred into a crucible, then put into an oven under air atmosphere and heated to 450°C at 10°C/min, kept at that temperature for 2 h and let cool down until room temperature was reached. The calcination under air atmosphere was carried out to eliminate any fatty acids capping the nanoparticles.

3.2 Electrode Fabrication

The components used in the electrode slurries were the synthesized active material (C-coated TiO_2 at 500, 600, or 700°C), along with carbon black (Super P) as an electronic enhancer and PVDF binder in a weight ratio of 8:1:1. The powders were grinded together in a mortar for 20 minutes and mixed in with 0.3 mL *N*-methyl-2-pyrrolidone (NMP) to form the slurries. To guarantee the homogeneity of the mixtures, a continuous stirring at room temperature was undergone for 3 h at a hot plate. The final slurries were drop casted on 12 mm diameter Cu foil substrate disks (0.25 mm thickness) and further dried at 80°C for 4 h under vacuum. The mass loading of active material was controlled to be 1.5 – 2.5 mg cm^{-2} on each electrode. To ensure a proper contact of the different materials, the electrodes were crimped with a pressure of 2 MPa.

3.3 Lithium Ion Coin Cell Assembly

The electrodes were built into CR2032-type coin cells in an argon-filled glove box after sitting in an oven at 70°C for 20 minutes to remove any moisture that could alter the electrochemical performance. The assembly consisted in a negative case topped with a metallic Lithium disk used as the counter electrode. Four drops or 40 µL of a 1 M $LiPF_6$ in ethylene carbonate and diethyl carbonate in a 1:1 by volume mixture electrolyte were dropped onto the Li disk and then topped with a Polypropylene-Polyethylene-Polypropylene (PP-PE-PP) trilayer membrane as the separator. Another four drops of the electrolyte would soak the separator and the manufactured C-coated TiO2 electrode, topped off with a positive case to finally enclose all the components (Figure 3.1). A hydraulic crimping machine was used to apply pressure to the ensemble and completely seal the coin cell.

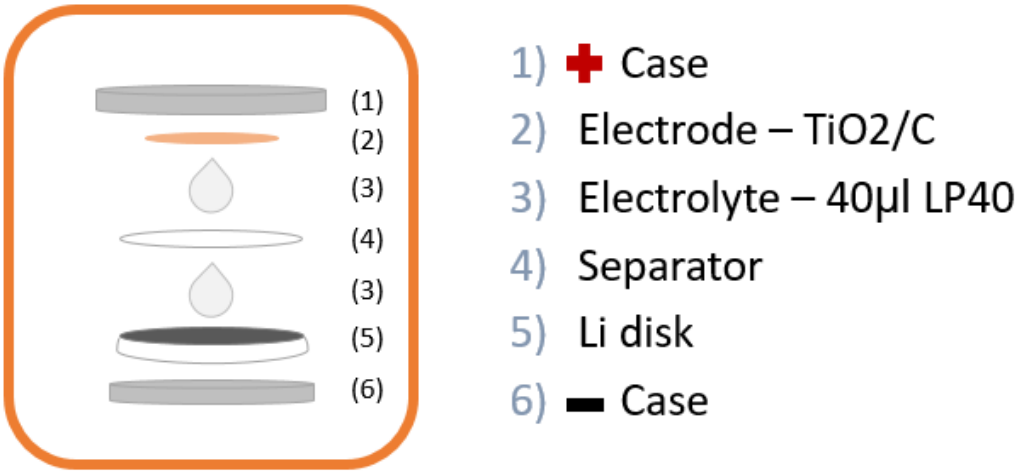

Figure 3.1. Scheme of the components of a Lithium coin cell.

3.4 Material and Electrode Characterization

Material Characterization

X-Ray Diffraction patterns were recorded on a PANalytical X'Pert Pro X-Ray powder diffractometer using copper $K\alpha$ radiation ($\lambda = 1.54$ Å). Nitrogen sorption isotherms were measured at 77 K with a Micrometrics ASAP 2020 analyzer. The samples were degassed in vacuum at 180°C for 3 h before measurements were taken. The specific surface areas were calculated by the Brunauer-Emmett-Teller (BET) method using the adsorption branch in the relative pressure range from 0.04 to 0.25. The pore size distributions (D_p) were derived from the adsorption branch using the Barett-Joyner-Halenda (BJH) model. Transmission Electron Microscopy (TEM) images were obtained by a Philips CM120 microscope operated at 120 kV.

Electrochemical Characterization

The electrochemical test such as the Galvanostatic charge/discharge measurements were performed on a LAND2000 battery cycler at different current densities over a voltage range of 1.0 – 2.8 V (V *vs.* Li/Li^+) for 100 cycles. The specific capacity is based on the total mass of TiO_2 and the C layer. Electrochemical Impedance Spectroscopy (EIS) measurements were conducted on a Solartron 1287 using a sinusoidal signal with an AC voltage in a frequency range between 1 MHz and 0.01 Hz at full charge with a perturbation amplitude of 5 mV on the cells at open circuit potential[28].

Chapter 4

Results & Discussion

Once a detailed description of the methods practiced on the materials to finally assemble the Lithium ion battery has been displayed, the next step is to study and analyze the results obtained from the different measurements that have been taken.

In Chapter 4, an extensive observation over the data collected has been done with a further discussion of the chemistry behind it. Foremost, a XRD of the pristine TiO_2, along with the C-coated TiO_2 annealed under 500, 600 and 700°C will be presented in order to study the structure and quality of the synthesized material. TEM images of the calcinated samples will be used as a support for the previous XRD data. Surface area information will be obtained with N_2 adsorption curves (BET), as well as a BJH study of the pore size distribution of both the N_2 annealed materials and the air sintered control sample for comparison purposes. Lastly, an electrochemical analysis discussing the Galvanostatic charge/discharge curves will be shared along with an EIS test to evaluate any improvements achieved by the manufactured Li-ion battery cells.

4.1 Composition and Structure Analysis

4.1.1 XRD and TEM

A good understanding of both structural and compositional features of the synthesized C-improved powders is necessary to further interpret any electrochemical data collected from the fabricated Li-ion coin cells. Having subjected pure nanosized TiO_2 to different temperatures to analyze its coating effects, an XRD on each of these calcinated black product powders has been compared to that of the pure, unaltered TiO_2 nanoparticles. Figure 4.1 displays the recorded XRD patterns of the C-coated TiO_2 sintered at 700, 600 and 500°C alongside the pristine Titania. For the sake of simplicity, the annealed powders have been named TiO_2@C-700, TiO_2@-600 and TiO_2@C-500, respectively.

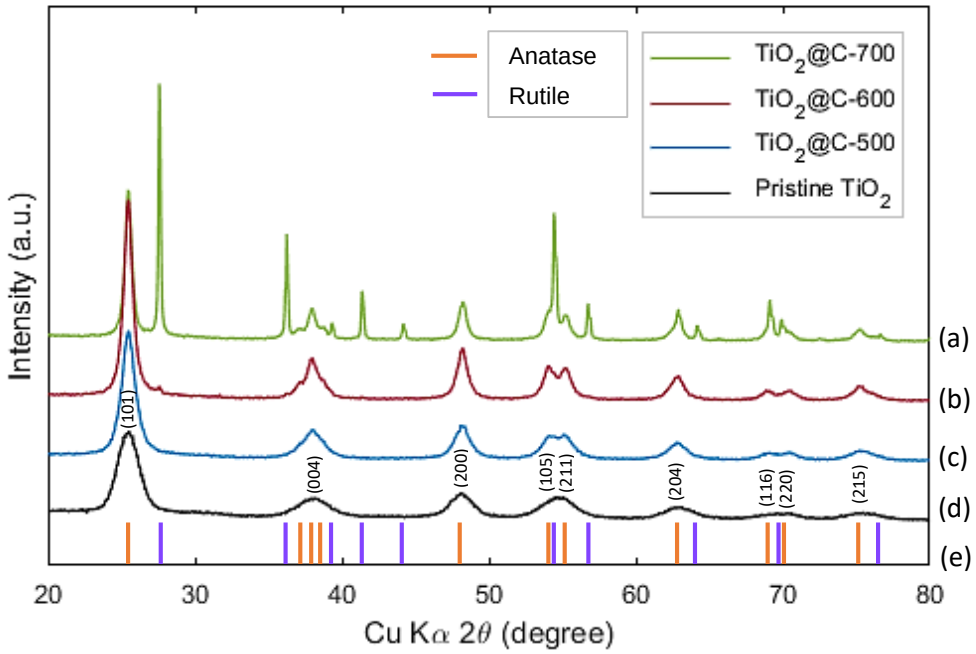

Figure 4.1. XRD patterns of the TiO_2 nanoparticles after N_2 annealing for 3 h under (a) 700°C, (b) 600°C, and (c) 500°C. (d) XRD pattern of Pristine TiO_2. (e) Position of the XRD peaks corresponding to anatase (orange) or rutile (purple) TiO_2 phases.

Comparing the patterns with the colored bars at the bottom (e), pristine TiO_2 shows a clear structure consisting of anatase only. The heating of the samples at lower temperatures such as 500°C doesn't significantly alter the structure giving clear anatase peaks on the XRD pattern. However, temperature does play an important role on the structural integrity of the TiO_2. Such effects start to peek through when heating the powder at 600°C, mostly consisting of anatase, but are completely visible on the 700°C heated nanoparticles, being dominant in both anatase and rutile phases.

The gradual transition from pure anatase to a mixture with rutile as the temperature of the annealing on the samples increases, suggests that the phase transformation – anatase to rutile – occurs during the heat treatment process (Fig. 4.1 (a), (b) and (c)). We can say that the phase transformation from metastable anatase to stable rutile takes places from 600°C to 700°C [29], were the most abrupt rutile phase peaks appear.

As explained in previous chapters, the convenience of working with an anatase structure in lithium ion batteries is of great interest due to further improved lithium intercalation which, in turn, leads to greater electrochemical performance. Knowing the crystallinity of the rutile phase, very poor intercalation with severe volume change would take place when subjecting such material under a constant voltage change. Thereby, the TiO_2@C-700 sample will not be a good candidate as anode material.

Further information can be extracted from the depicted figure, such as the (002) graphitic peak not being visible on the annealed samples. That strongly suggests the presence of long-range amorphous graphitic structure in the C-coated TiO_2 particles that is lost in these samples. Moreover, the broadening of the peaks, mostly in the case of the pristine TiO_2 and the TiO_2@C-500, indicates a smaller crystallite size that can be estimated from the XRD peaks using the Scherrer equation (Eq. 4.1).

$$B(2\theta) = \frac{K\lambda}{L\cos\theta} \quad (4.1)$$

Where K is the Scherrer constant (0.94 for spherical crystallites with cubic symmetry); λ is the X-ray wavelength and is equal to 1.54178 Å; θ is the XRD peak position; B is the FWHM of the XRD peak, and L is the crystallite size.

One can observe the XRD peak broadens as the crystallite size gets smaller (B varies inversely with L). Thereby, the XRD patterns in Fig.4.1 suggest a change in size from the pristine TiO_2 synthesized nanoparticles with respect to the sintered powders. Such diameter change can give rise to the appearance of the graphitic-like layer covering the crystallites. The parameters required in Eq. 4.1 are collected in the following tables, estimating different diameter sizes for the pristine Titania, TiO2@C-500 and TiO2@C-600 (TiO2@C-700 has been excluded due to non-necessity).

Pristine TiO_2

Peak position 2θ (°)	25.5	38.07	48.15	54.63	54.99	62.94	69.58	70.54	75.4
FWHM B_{size} (°)	1.71	2.68	1.97	2.63	2.63	2.33	2.48	2.48	2.18
Particle diameter (nm)	4.98	3.28	4.62	3.55	3.56	4.18	4.08	4.10	4.81

Table 4.1. Parameters collected from Pristine TiO_2 XRD pattern (Fig. 4.1(d)) and estimated crystallite diameter size using Scherrer Equation.

TiO_2@C-500

Peak position 2θ (°)	25.50	37.91	48.2	54.18	55.19	62.79	69.12	70.39	75.35
FWHM B_{size} (°)	1.16	1.67	1.22	2.43	2.43	1.47	2.59	2.59	1.82
Particle diameter (nm)	7.34	5.26	7.46	3.84	3.86	6.62	3.89	3.92	5.76

Table 4.2. Parameters collected from TiO_2@C-500 XRD pattern (Fig. 4.1(c)) and estimated crystallite diameter size using Scherrer Equation.

TiO_2@C-600

Peak position 2θ (°)	25.45	37.91	48.25	54.08	55.24	62.89	68.92	70.49	75.25
FWHM B_{size} (°)	0.81	1.57	0.91	1.06	1.02	1.07	1.17	1.26	1.42
Particle diameter (nm)	10.51	5.59	10.00	8.80	9.19	9.10	8.61	8.07	7.38

Table 4.3. Parameters collected from TiO_2@C-600 XRD pattern (Fig. 4.1(b)) and estimated crystallite diameter size using Scherrer Equation.

In Table 4.1., crystallite diameters ranging from 3.5 nm to nearly 5 nm give an estimated average particle size of 4.13 nm for the pristine TiO_2. In Table 4.2., diameter sizes have slightly increased after the heating treatment at 500ºC of the crystallites, which suggests that increment in might be related to the formation of a graphitic-like layer coating the nanoparticle. The average diameter is 5.3 nm, which compared to that of 4.13 nm in pristine, can help estimate the thickness of the C coating. Typically, a single layer of graphene is reported to be between 0.4 to 1.7 nm thick[30]. Comparing both crystallite dimensions, the difference in size can be given by the presence of a monolayer of carbon material in a core-shell TiO_2@C particle structure. Finally, in Table 4.3., not much information regarding the particle size can be extracted from the estimated diameters, since these seem to not follow one size or another, but they rather show a more aggregation-like distribution.

Compared to commercial TiO_2 (P25 is around 30 nm in diameter), which typically consists of a combination of rutile and anatase, the two-phase method approached in the synthesis of nanostructured TiO_2 particles has successfully produced pure 4nm-anatase TiO_2 (Fig. 4.1(d)), lending future research a trustworthy, cheap and simple recipe for larger scale, smaller size titania production.

The TEM images (Fig. 4.2) show the carbon coated TiO_2 powder with crystal size of around 5 to 6 nm, as estimated in TiO_2@C-500 TEM according to the scale bar (Fig.4.2 (a-b)). Spherical-like nanocrystals are observed in TiO_2@C-500, however, smoother lines are shown in the case of TiO_2@C-600 (Fig.4.2 (c-d)) indicating the presence of particle agglomeration due to heat treatment.

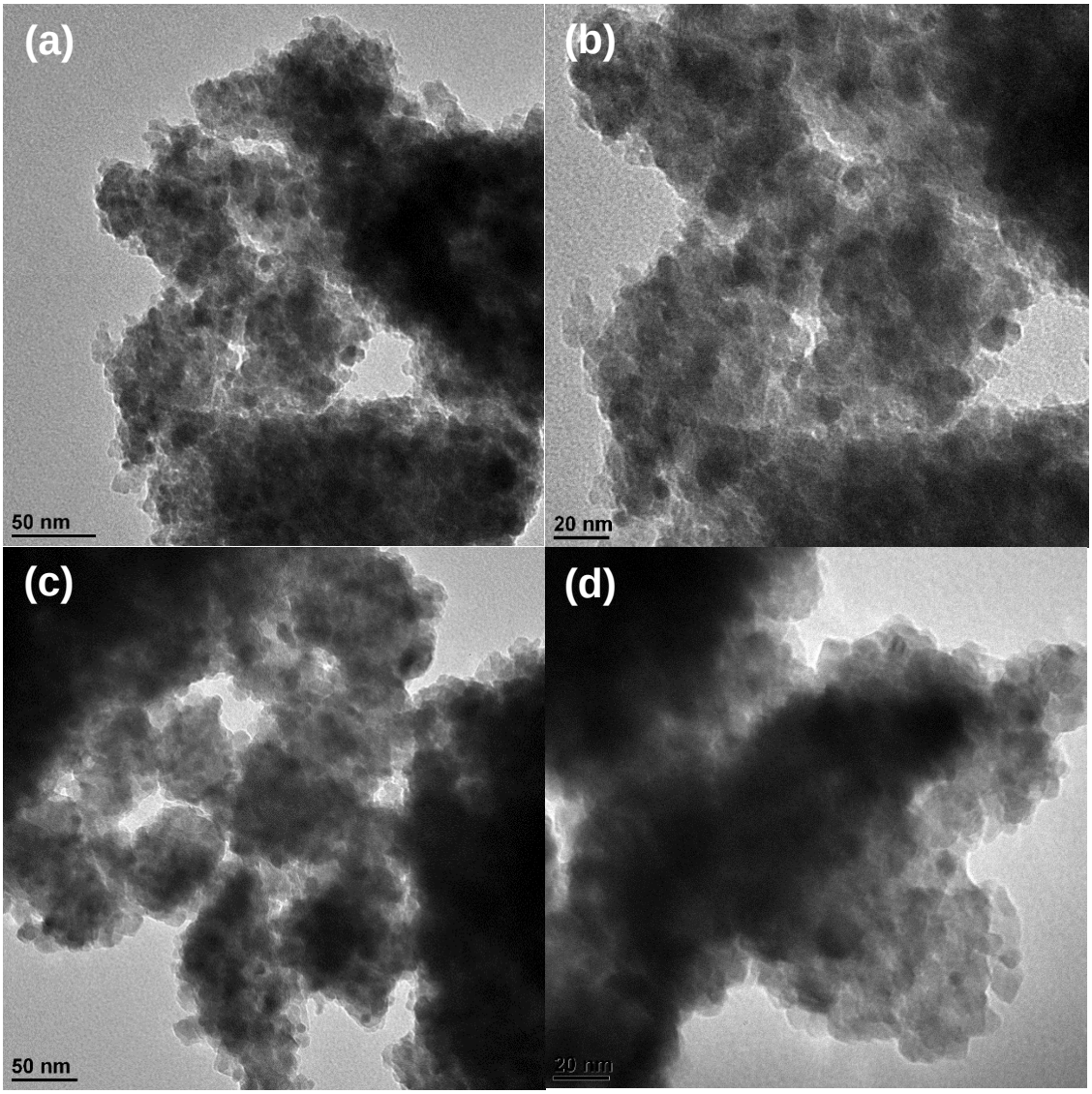

Figure 4.2. (a) and (b) TEM images of the synthesized C-coated TiO_2 nanoparticles under N_2 annealing at 500°C at different magnifications; (c) and (d) TEM images of the 600°C N_2 annealed core-shell TiO_2. The scale bars in (a) and (c) refer to 50 nm, and those in (b) and (d), to 20 nm.

The images are consistent with the XRD data in Figure 4.1 regarding aggregation at higher sintering temperatures, as well as the crystallite size images as backing of the estimated values obtained in Eq. 4.1. No ultimate information could be extracted from the TiO_2@C-600 XRD pattern like it did in the TiO_2@C-700 case; however, the TEM images have confirmed the beginning of structural changes when annealing at temperatures of 600°C and above. Working with smaller nanocomposites, increased side reactions are expected to happen since nanostructuring gives rise to a more reactive material. Nonetheless, at a right heating temperature, carbon coating can prevent particle agglomeration normally experienced when nanostructuring material.

4.1.2 BET – Surface Area

After a successful carbon coating of the nanocrystals, N_2 adsorption-desorption isotherms were collected in Figure 4.3 to confirm any improvements in the porous nature of the core-shell mesoporous TiO_2 particles after the respective 500°C and 600°C N_2 atmosphere annealing.

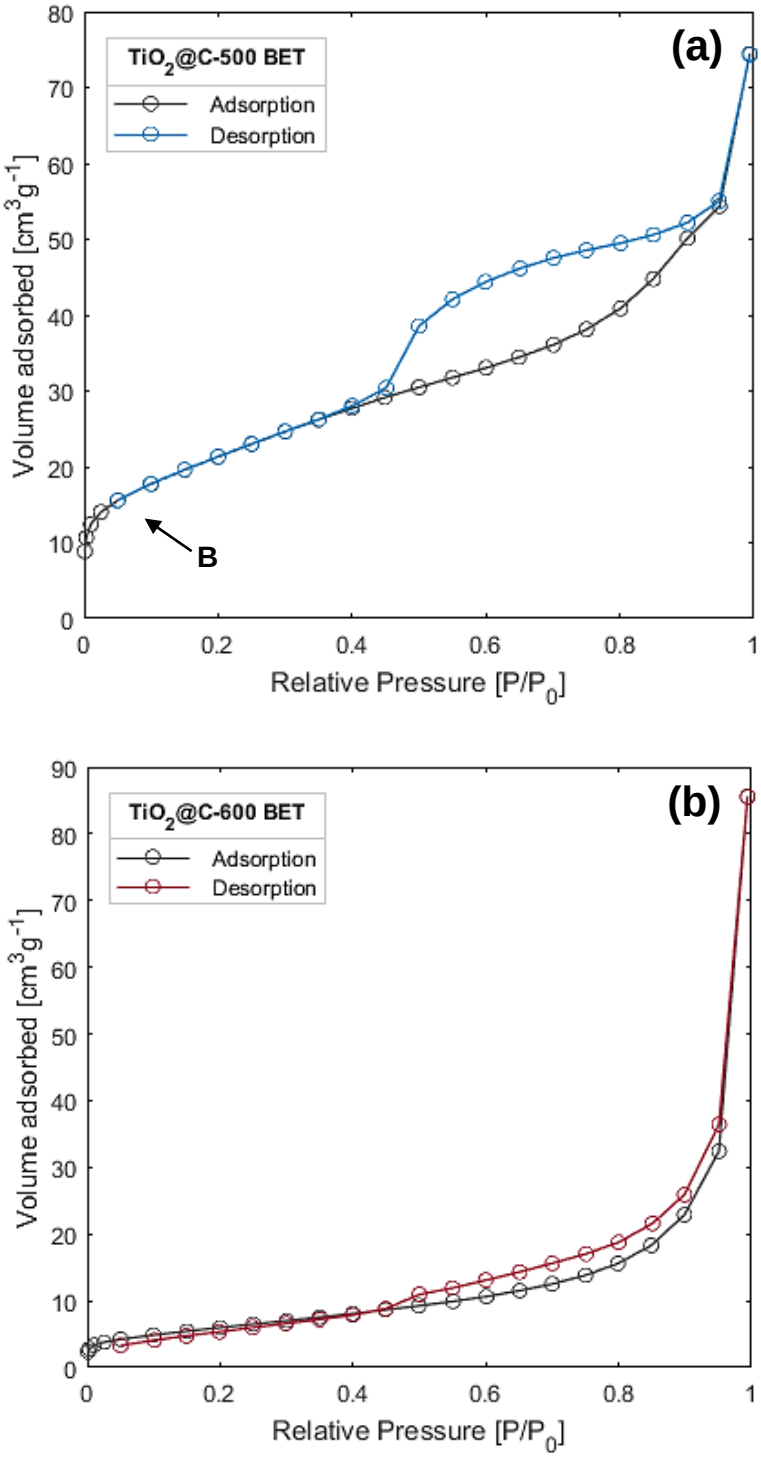

Figure 4.3. Nitrogen sorption isotherms of (a) TiO_2@C-500 and (b) TiO_2@C-600 nanocomposites.

The crystalline TiO_2 nanocomposites calcinated at 500°C show a clear type-IV isotherm (Fig. 4.3(a)) with a Brunauer-Emmett-Teller (BET) surface area of 76 $m^2 g^{-1}$. Such value has already improved with respect to those of previous research in non-carbon coated hierarchical TiO_2 nanostructures [30] [31].

A mesoporous configuration is generated by the arrangement of the carbon and the TiO_2, which is represented in Figure 4.3 by the hysteresis at a relatively low relative pressure of 0.45, in both cases. Nevertheless, a very different volume is adsorbed when comparing Fig. 4.3(a) and (b). Point B in (a) shows the adsorption of a monolayer of N_2 on the porous material. At relative pressures above that of the monolayer formation, the smaller pores start to build up multilayers and slowly filling up, and so are larger pores as the pressure increases. That is due to capillary condensation of the N_2 within the porous material[32]. Saturation takes places when P/P^0 is nearly 1.0, when the integrity of the porous material contains condensed nitrogen, so that the volume of bulk liquid nitrogen is that same volume inside the pores.

Knowing this, a hysteresis centered at lower relative pressures indicates a mesoporous structure. In that case, (a) isotherm shown in Figure 4.3 represent that of a mesoporous material; whereas (b) is curved near the saturation point at very low volume adsorption values, indicating lower porosity and a not-so-defined pore size distribution, meaning there might be aggregation, unlike in (a). The N_2 sorption isotherm of TiO_2@C-600 confirms a low surface area of 20 $m^2 g^{-1}$.

4.1.3 BJH – Pore Size Distribution

Barrett-Joyner-Halenda (BJH) method was used to determine the pore size distribution obtained from the previous seen nitrogen sorption isotherms. Figure 4.4 confirms the speculations made regarding the placement of the hysteresis and its shape in the BET representations. A narrow pore size distribution is placed at 1.17 nm and 3.96 nm as seen in Figure 4.4(a) for TiO_2@C-500. The BJH data is consistent with that provided by the BET, which suggested a defined and rather small pore size distribution. At the same time, Fig. 4.4(b) also confirms a broader distribution peak at 3.79 nm, as well as an undefined pore distribution of a variety of sizes, showing the agglomeration observed from the TEM images and the BET.

All in all, good results have been obtained from synthesizing nanostructured TiO_2 composites through this two-phase hydrothermal method. Giving both a high yield of around 92% to 98% – promising for larger scale production –, and the structure, size and porosity that were expected to be enhanced.

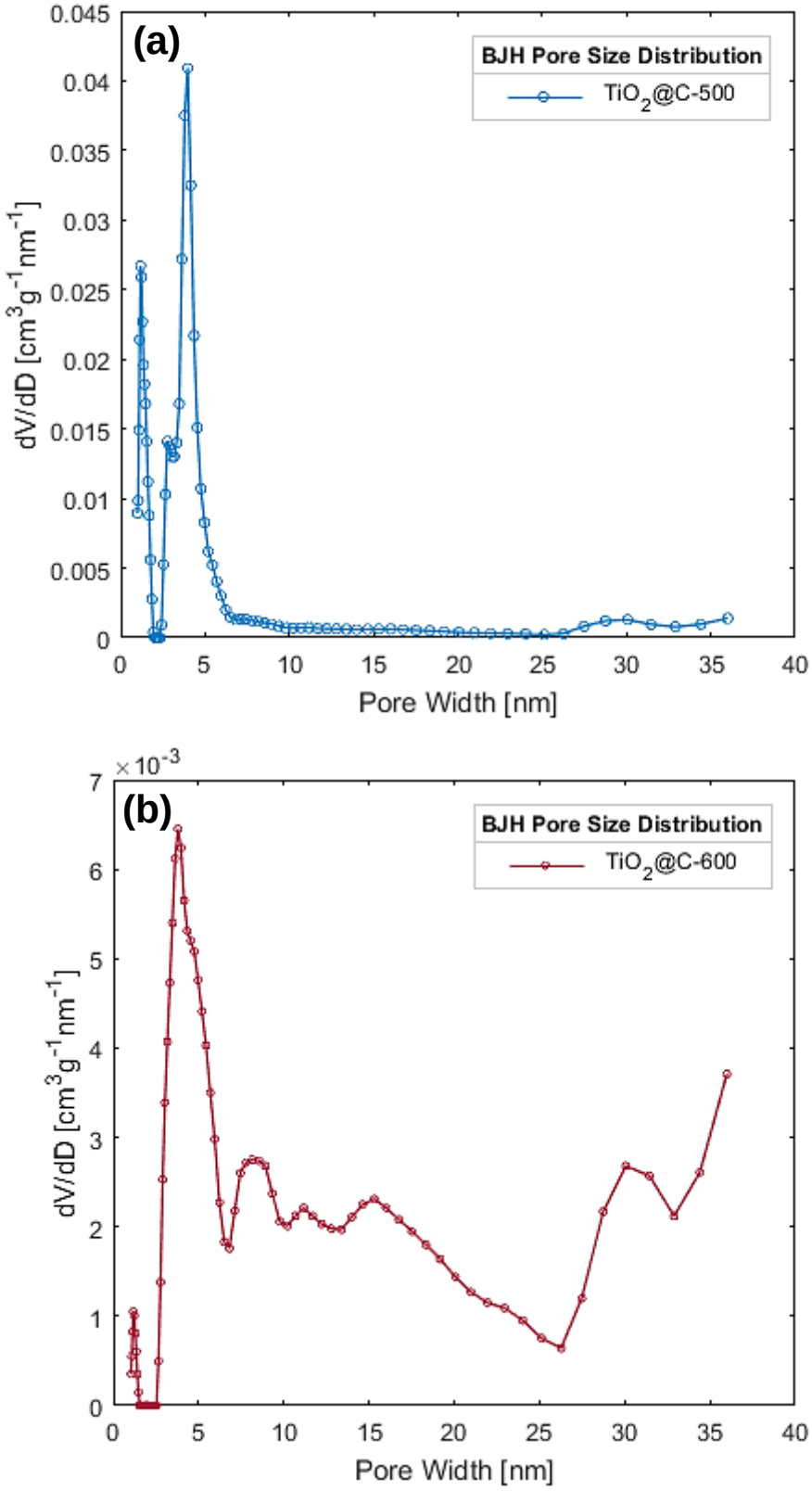

Figure 4.4. BJH Pore Size Distribution of (a) TiO_2@C-500 and (b) TiO_2@C-600 nanocomposites.

4.2 Electrochemical Analysis

The previous characterization results have confirmed so far the synthesis of quality mesoporous core-shell TiO_2 nanocomposites, which provide a better surface area resulting in larger interfacial contact of the anode active material with the electrolyte, so the kinetics during charge-discharge will be enhanced and a better intercalation of Li ions will take place in the material surface rather than in the bulk. More intercalation on the surface implies a faster ion diffusion, which is key for good performance in higher density current or high-rate battery cycling. An electrochemical analysis has then been conducted in order to test how well the coating effect helps improve the material's conductivity compared to a non-carbon coated TiO_2 control sample, as well as the downsizing contribution to the enhanced anode properties in comparison to commercial TiO_2 (P25) assembled coin cells.

4.2.1 Galvanostatic Charge/Discharge Measurements

The electrochemical performances of the as-prepared TiO_2@C nanoparticles at different calcination temperatures (500, 600, and 700°C) were investigated and the typical galvanostatic charge-discharge curves (GC) of the obtained TiO_2@C were shown in Figure 4.5. In each of the cases, the potential curves were obtained at a current density of 0.1C on the 1st cycle for activation of the cell, and then maintained at 1C until the 100th cycle.

Recalling the Li intercalation/deintercalation reaction in TiO_2 seen in Chapter 2, Eq. 2.1.:

$$xLi^+ + xe^- + TiO_2 \rightarrow Li_xTiO_2 \quad (2.1)$$

Working with anatase TiO_2, regardless of any later coating, the theoretical Li ion insertion $x = 0.5$ (corresponding to a capacity $C_x = 167\ mA\ g^{-1}$) increases to $x = 0.6$, or higher, due to favorable Li ion insertion within the anatase matrix[33]. Following the so-known theoretical capacity expression:

$$C_x = \frac{x \cdot F}{M_w(TiO_2) \cdot 3.6} \quad (4.2)$$

For $x = 0.6$, $F = 96485\ C/mol$, and $M_w(TiO_2) = 79.87\ g/mol$, the value of the theoretical capacity is now $C_x = 200\ mA\ g^{-1}$. This value will be used in all the electrochemical measurements conducted in this experiment. Keeping that in mind, the corresponding current densities applied to the GC tests are 20 mA g^{-1} for 0.1C rate, and 200 mA g^{-1} for 1C. Moreover, the voltage range in these measurements was 1.0 – 2.8 V (V *vs.* Li/Li^+).

Also, it is worth mentioning a controlled mass loading of about 2.2 mg cm^{-2} (±0.2) of the active material on the electrode, since it can strongly affect the electrochemical performance. Such value is in the range of previous studied high-rate nanostructured TiO_2 anodes[34].

Figure 4.5 illustrates the galvanostatic charge-discharge curves of TiO_2@C-500 – based electrode. Two large voltage plateaus are observed for the discharging and charging processes, at 1.7 V and 1.89 V respectively. The presence of the plateau region alongside the discharge and charge slopes, suggest the lithium insertion process to be divided in three stages[35]:

Stage 1: in the discharge curve, an abrupt slope from the open circuit voltage potential at 2.8 V shows a high decrease to a voltage of 1.7 V. This region corresponds to the storage of 0.15 mol Li^+ per mol of TiO_2 related to the insertion of nearly a monolayer of Li ions covering the TiO_2@C nanospheres[36 37].

Stage 2: or plateau region, is attributed to the phase transition of TiO_2 between the tetragonal and orthorhombic phases when the TiO_2 crystal structural voids are occupied by the Li ions during insertion. It is observed a capacity of roughly 50 $mA{\cdot}h{\cdot}g^{-1}$, corresponding to this plateau.

Stage 3: consists on the Li ion insertion into the surface of the anode material after the plateau region, where a gradual voltage decrease takes place. This slope region contributes a capacity of around 187 $mAh{\cdot}g^{-1}$, indicating high surface insertion values which active sites have been successfully improved with smaller-sized nanoparticles and conductivity enhancement with carbon coating[38].

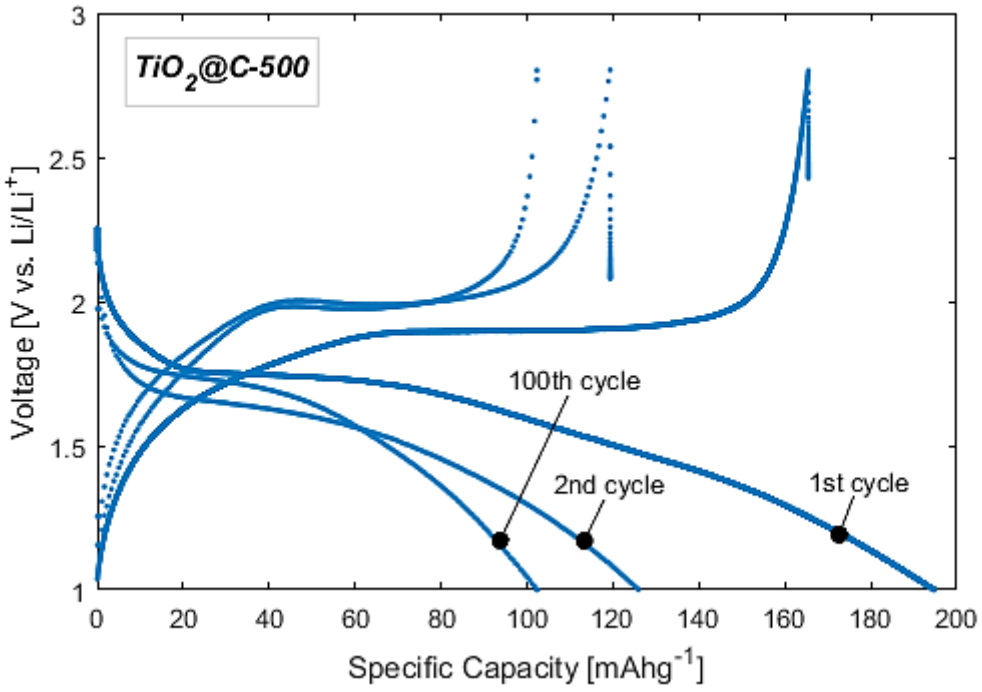

Figure 4.5. Typical galvanostatic charge-discharge 1st, 2nd and 100th cycle curves of the mesoporous nanostructured C-coated TiO_2 crystallites sintered at 500°C, at 0.1C rate (1st cycle) and 1C rate (from 2nd to 100th cycle).

A first discharge and charge capacity of 194.8 $mAh \cdot g^{-1}$ and 165.5 $mAh \cdot g^{-1}$, respectively, are achieved during the insertion/extraction process. This irreversible behavior is translated to a capacity loss in the first cycle of 29.3 $mAh \cdot g^{-1}$ which, in turn, corresponds to a very high first coulombic efficiency of 85% (extraction/insertion ratio)[39]]. Since the working range potential is always larger than a voltage of 1.0 V, no electrolyte reduction should be deduced from this capacity loss[40]. Notice that the first discharge capacity corresponds to 0.59 mol Li^+ out of the 0.6 we estimated for Li_xTiO_2.

From the second cycle, a discharge capacity of 125.9 $mAh \cdot g^{-1}$ is obtained, despite having decreased respect to that on the first cycle, a corresponding charge capacity of 119.4 $mAh \cdot g^{-1}$ indicates an increased coulombic efficiency of the 95%, which keeps increasing up to a 99.9% when in the 100th cycle. Besides, from the 20th cycle until the cycling is finished, a retention of 94% of the capacity is achieved. Thus, showing outstanding robustness and electrochemical stability. A reason for the irreversible capacity loss to decrease so rapidly upon cycling may be due to the trapping of the Li ions in the irreversible anatase vacancies during the first cycle, which remain in those sites for the ongoing cycles and let the proper reversible reaction to occur. Moreover, the fact that the diffusion-controlled capacity region, or plateau, diminishes when increasing from 0.1C to 1C, suggests that at higher rates very low diffusion will take place in the TiO_2 material framework. Thus, the surface capacity contribution will become more dominant at higher current densities.

These same observations can be done in Figure 4.6. One can see for TiO_2@C-600 (Fig. 4.6(a)) a lower first discharge capacity, 165 $mAh \cdot g^{-1}$, compared to that of TiO_2@C-500. In this case, it only represents an intercalation value of the 50%, or x = 0.5. The decreased capacity for the 600°C annealed nanoparticles reinforce the BET and pore size distribution data confirming a clearly lower surface area for the Li ions to be inserted during the discharge process. However, a good first coulombic efficiency of 88% is reached. The shape of the 2nd to 100th cycle curves demonstrate mostly surface contribution for Li ions insertion having lost the 46% of the capacity from the first cycle. The good properties of having nanostructured the anode material increasing the surface area, as well as the C-coating have still given decent results at cycle 1, nonetheless, the particle aggregation keeps the battery cell from performing well in the long run.

The presence of rutile phase within the structure of TiO_2@C-700 shows the instability when using it as a potential anode material (Fig. 4.6(b)). Three plateau regions are depicted in the 1st discharge curve. The one at 1.75 V is due to Li intercalation on the anatase TiO_2 structure when the phase transition between the tetragonal and orthorhombic phases occur. The other plateau regions are attributed to the rutile phase of the TiO_2 during lithiation, when the original rutile structure is rearranged at 1.4 V to its lithiated form, and then to a layered structure at 1.25 V [41].

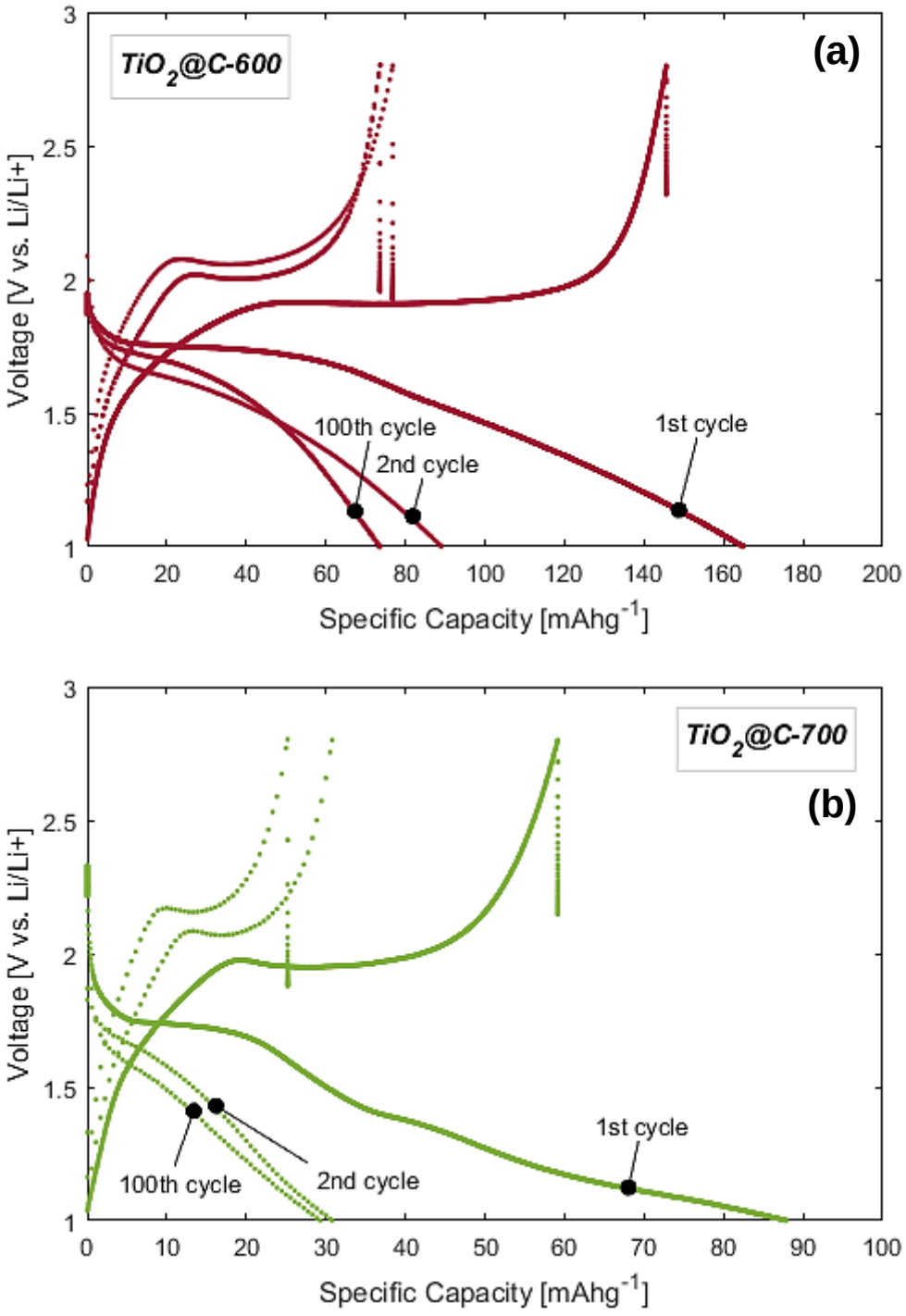

Figure 4.6. Typical galvanostatic charge-discharge 1st, 2nd and 100th cycle curves of the mesoporous nanostructured C-coated TiO_2 crystallites sintered at (a) 600°C and (b) 700°C, at 0.1C rate (1st cycle) and 1C rate (from 2nd to 100th cycle).

Figure 4.6(b) shows a very bad performance of the TiO_2@C-700 material as speculated from the first XRD patterns obtained of the sample. From 2nd to 100th cycles a great capacity loss takes place, suggesting a very large irreversibility and the likelihood of it being due to the SEI formation[42].

After the study of the suitability of C-coated TiO_2 nanospheres at different annealing temperatures, two control electrodes have been manufactured for the sake of experiment completion. Thereby, the corresponding electrochemical analysis have been conducted to:

Control 1: Size effect. Assembled coin cell with built-in Commercial TiO_2 (P25, 30 nm diameter) based electrode.

Control 2: Coating effect. Mesoporous nanostructured C-free TiO_2 crystallites (sintered under air atmosphere at 450°C) based electrode assembled in a coin cell.

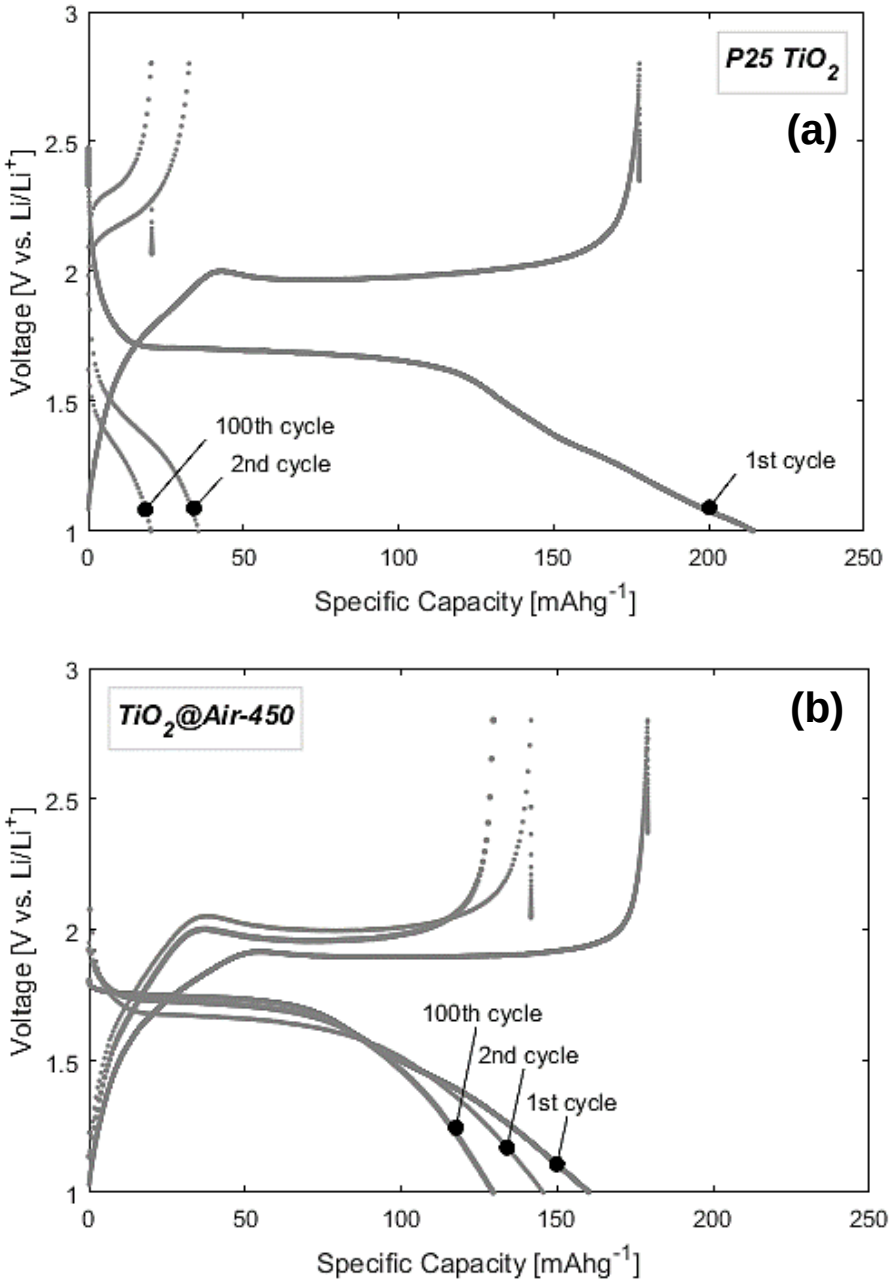

Figure 4.7. Galvanostatic charge-discharge 1st, 2nd and 100th cycle curves of (a) commercial TiO_2 P25 self-assembled coin cells, and (b) C-free TiO_2 crystallites air sintered at 450°C, at 0.1C rate (1st cycle) and 1C rate (from 2nd to 100th cycle).

Figure 4.7(a) illustrates the reason why extensive research in Lithium ion battery is of need. A very good first discharge capacity value of 214.4 $mAh \cdot g^{-1}$ P25 excels that of the as-synthesized TiO_2@C-500 electrode, experiencing a Li insertion of x = 0.65. With a first charge capacity of 177.6 $mAh \cdot g^{-1}$ the corresponding coulombic efficiency is an 82%. However, the capacity loss observed from the 2nd cycle onwards reaches the 84%, attributing the assembled battery cell a really bad cycle life and stability, as well as the non-suitability for high current density performance.

The galvanostatic charge-discharge curves of TiO_2@Air-450 in Figure 4.7(b) show a greater first charge capacity than discharge capacity of 178.9 $mAh \cdot g^{-1}$ and 160.2 $mAh \cdot g^{-1}$ respectively. Thus, surprisingly giving a coulombic efficiency of 111.6%. This can be ascribed to an electrode being lithiated taking less Li ions than the amount released when delithiated[43]. For this to happen, nanosized particles are more likely to have higher reaction activity as well as an improved surface area that enlarges the contact area exposed to intercalation/deintercalation. Despite this effect only taking place on the first cycle, a 97% coulombic efficiency is depicted on the 2nd cycle, and a good capacity retention of 92% is observed from the 10th cycle onwards, which suggests a good stability of the non-carbon-coated TiO_2 nanoparticles.

Coating effects – comparing TiO_2@Air-450 with TiO_2@C-500 – are clearly observed not only on the first discharge and charge capacity values, but also the shape of the discharge curves. A more abrupt slope after the plateau region with a capacity contribution of around 60 $mAh \cdot g^{-1}$ implies a poorer surface area and most of the Li ions insertion to be at bulk level. Thus, not making it eligible for higher rate performances.

Size effects can be studied from a P25 ($\sim 30\ nm$) and a TiO_2@Air-450 ($\sim 4nm$) comparison. The most obvious improvement observed when nanosizing the material is the enhancement of the surface area and, thus, the active sites available for Li ion insertion. So an important ratio of the intercalation takes place at surface level and increasing the current density from 0.1C to 1C doesn't affect the performance of the cell.

4.2.2 Electrochemical Impedance Spectroscopy (EIS)

Further insight on the electrochemical performance is given by the EIS measurements. The Nyquist plots shown in Figure 4.8 will allow a kinetics analysis of the performances for each of the electrode materials. The bellow depicted figure illustrates the Nyquist plots after 100 cycles. Here TiO_2@Air-450, TiO_2@C-500, TiO_2@C-600 and TiO_2@C-700, are named T450A, T500C, T600C and T700C, respectively.

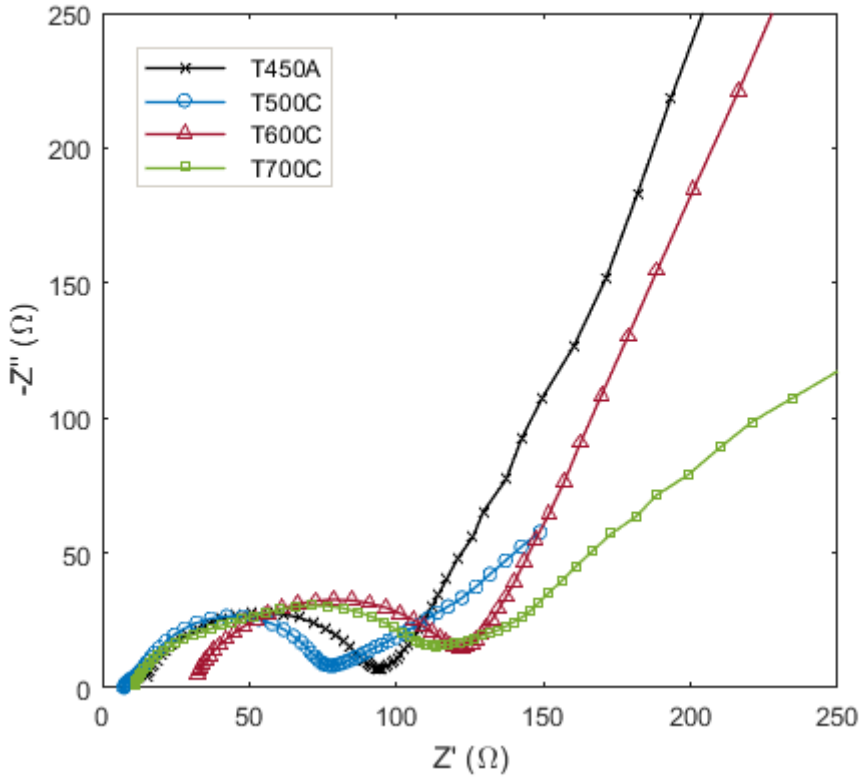

Figure 4.8. Nyquist plots of the electrodes composed of the as-synthesized air-sintered carbon-free TiO_2 (T450A), and the N_2 annealed carbon-coated TiO_2 at 500, 600 and 700°C (T500C, T600C, and T700C, respectively).

Every EIS spectrum shows three differentiated regions: high frequency, related to Li ion diffusion through the surface layer; medium frequency, that of charge transfer reaction, and low frequency, corresponding to the cell geometric capacitance, or the so called Warburg tail[44].

To see the internal resistance of the electrode and the electrolyte in the battery, that value is given by the intercept at the Z' axis. Thus, T600C, having the largest internal resistance may refer to the great capacity loss from the 1st to the 2nd cycle.

Moreover, the semicircle diameter at high frequencies is the measurement of the Li^+-charge transfer impedance, which is clearly larger for T450A, T600C and T700C, with 95 Ω, 90 Ω and 100 Ω, respectively.

These higher Li^+ charge transfer impedance and, thus, a poorer Li ion transportation, can be ascribed to the lack of a carbonaceous layer on the nanoparticles to enhance both conductivity and active site at surface level in the case of T450A; for T600C, the formation of aggregated nanoparticles counteracting the purpose of downsizing the crystallites for improved surface area and Li diffusion; and for T700C, the presence of rutile phase, showing a poorer Li intercalation due to its compact structure. Nevertheless, a smaller charge transfer impedance is shown compared to that of commercial TiO_2 (Fig. 4.9(a)). T500C having a 70 Ω charge transfer impedance is still not the lowest that has been reported up to date, however, it comes to an agreement when comparing it to the other three electrode materials, showing a better Li ion diffusion due to a better quality mesoporous nanostructure.

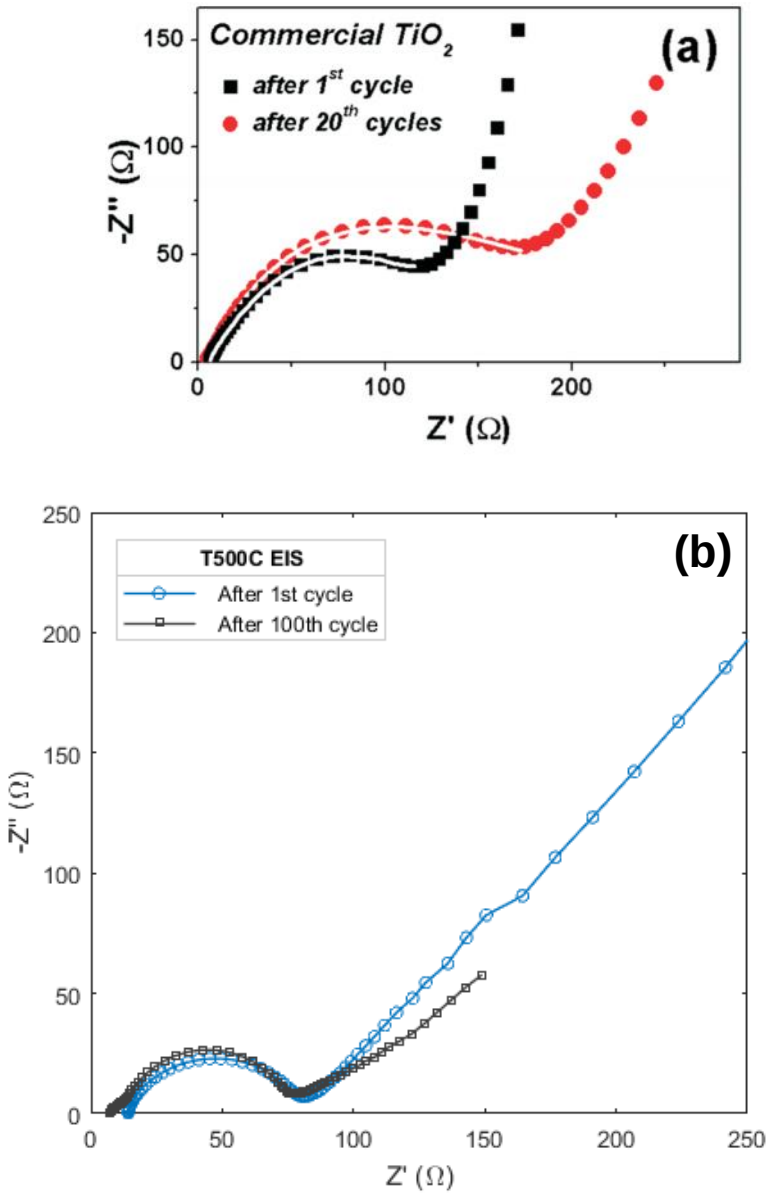

Figure 4.9. Nyquist plots comparing 1st to 100th cycle impedance changes in (a) Commercial TiO_2-based electrodes; and in (b) TiO_2@C-500-based electrodes (T500C).

The slope effect, or Warburg tail, is more clearly depicted in Figure 4.9, where the before and after comparison has been presented for kinetic analysis. From (a) and (b) it is observed the tendency after cycling is a decrease in the low frequency slope. That is related to the capacitance and is translated to a diminished rate performance[45].

The biggest difference between the P25 and the T500C, however, is not only the obvious smaller charge transfer impedance, but also the consistent semicircle diameter size in T500C even after 100 cycles – from 66 Ω to 70 Ω –, implying a well retained capacity throughout the cycling process even when increasing the rate performance from 0.1C to 1C, as well as a consistent, stable, quality porous matrix that is minimally affected by the rocking chair process of insertion and desertion. The non-increment of the charge transfer impedance and, thereby, the maintenance of a Li ion diffusion between electrode and electrolyte, indicates the effectiveness of the carbon coating avoiding the formation of a SEI layer, a well improved surface area where most of the intercalation/deintercalation occurs, and a promising long-cycle-life electrode material.

Chapter 5

Conclusions & Further Research

The overall of these results clearly demonstrate the nanosizing of structured crystallites does not only provide the material with improved surface area or porosity, but it also gives rise to more reactive material that might cause aggregation. It has been demonstrated the two-phase hydrothermal technique produces one order of magnitude smaller TiO_2 nanoparticles than the commercial material. Such technique uses easy-to-get, cheap materials and works at very settle conditions (decent temperature). Moreover, with a yield of the 92%-98%, this method might be suitable for larger scale production.

Regarding the enhancement of the titania poor properties, mostly very low conductivity, a good approach to overcome that matter, among many others, has been carbon coating of the as-synthesized anatase TiO_2 nanoparticles under N_2 atmosphere at 500°C. At higher annealing temperatures, the structure starts to aggregate because of increased reactivity and, at a certain point (700°C), rutile TiO_2 phase is found in the material's framework.

Ultrasmall nanoparticles have been found to show a better coulombic efficiency than commercial P25, indicating more capacity retention and, thus, a longer cycle life. Also, the GC results have shown an improved specific capacity compared to the theoretical value for TiO_2, a better cyclability, and a good capacity retention when increasing the current density. That could also be contrasted with the EIS test where smaller nanoparticles have shown more than half the charge transfer impedance commercial P25 has. Thus, nanosizing has successfully improved the Li diffusion within the cell, making it suitable for higher-rate performance.

Finally, the coating effect has also shown its improvements on the material. A higher specific capacity on carbon coated TiO_2@C-500, higher coulombic efficiency after 100 cycles, and a lower charge transfer and internal impedances proving, once more, the enhanced Lithium intercalation within the matrix due to a successfully synthesized ultrasmall mesoporous core-shell carbon-coated anatase TiO_2 nanoparticles.

There is a clear improvement of the material when coating with carbon to enhance its conductivity, as well as when nanostructuring to achieve greater surface area values for better Lithium insertion and shorter diffusion length.

However, a lot of work has yet to be done. Further characterization might be of great help to better understand the data collected from the electrochemical measurements. Cyclic Voltammetry tests might be a good addition, as well as cycling the battery cells for a higher number of cycles to prove their long cycle life. Also, higher rates can be applied to the cycling process to compare how much of the capacity can still be retained and how reversible these reactions are.

Following the line of the annealed temperatures under nitrogen, an interesting study could be that of TiO_2@C-400 nanoparticles. In fact, a quick sample was synthesized and annealed at 400°C and further tested showing the following TEM images and GC:

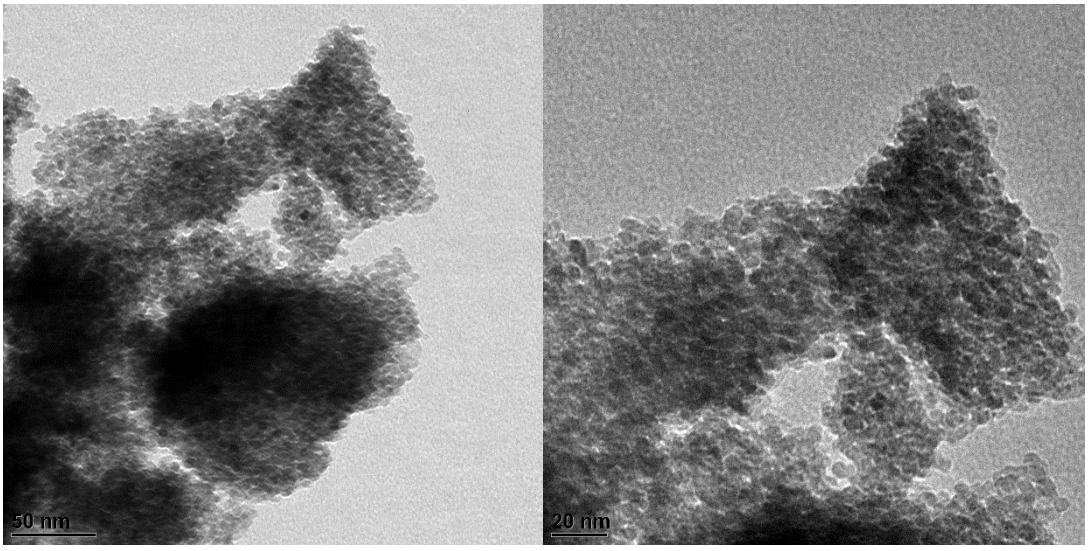

Figure 5.1. TEM image of TiO_2@C-400.

Clearer spherical-like nanoparticles are observed from the TEM images. A 4 nm particle size can be estimated and a successful C coating has been done due to the apparent inexistent signs of particle aggregation.

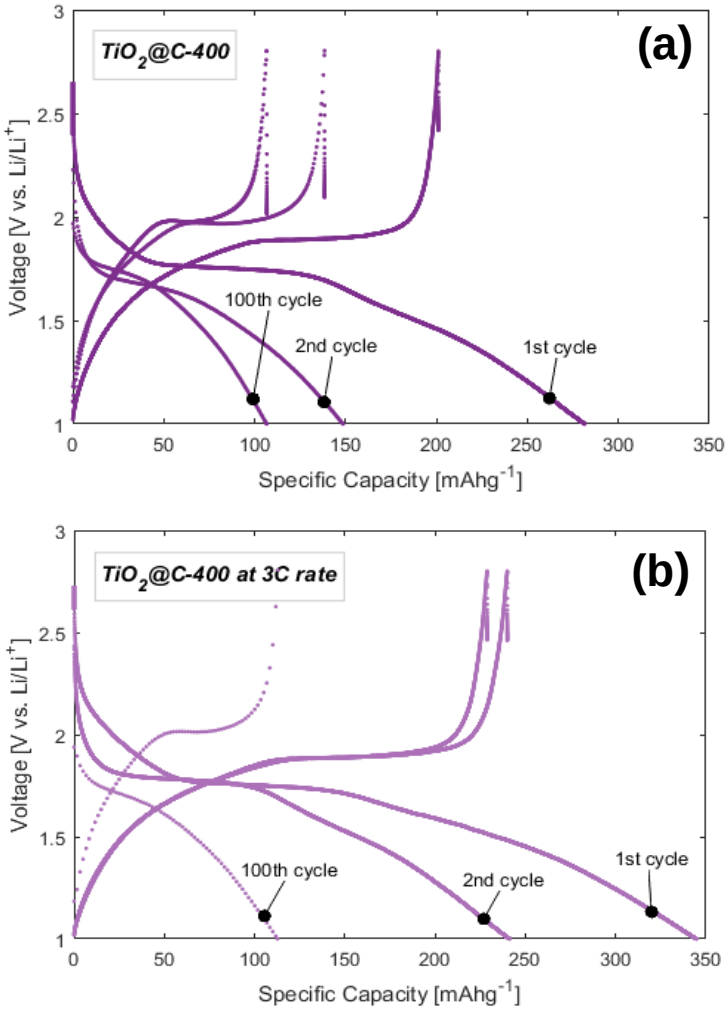

Figure 5.2. GC of (a) TiO_2@C-400 at 0.1C on 1st cycle, and 1C from 2nd to 100th cycle. (b) TiO_2@C-400 at 0.1C for 1st and 2nd cycles, and 3C until 100th cycle.

Very good specific capacities of 294 mAh·g^{-1} (a) and 344.7 mAh·g^{-1} (b) are observed. However, a large capacity loss is shown in Fig. 5.2(a) for the first to second discharge curves, which might need further insight and study. All in all, a good research material that could lead to further improvement of lithium ion batteries.

Bibliography

[1] Tirado, J.L. Materials Science and Engineering R 40 (2003) 103-136

[2] Jabbour, L., Bongiovanni, R., Chaussy, D. et al. Cellulose (2013) 20: 1523.

[3] G.E. Products, Rechargeable Batteries Applications Handbook, Elsevier Science1998.

[4] Scrosati B, Garche J (2010) Lithium batteries: status, prospects and future. J Power Sources 195:2419–2430.

[5] C. de las Casas, W. Li, A review of application of carbon nanotubes for lithium ion battery anode material, Journal of Power Sources, 208 (2012) 74-85.

[6] G.X. Wang, D.H. Bradhurst, S.X. Dou, H.K. Liu, Structural and electrochemical characteristics of Li1+x Mn2–x O4 and LiMn2 O4 for Secondary Lithium batteries., Battery Conference on Applications and Advances, 1998., The Thirteenth Annual, 1998, pp. 375-380.

[7] J.W. Fergus, Recent developments in cathode materials for lithium ion batteries, Journal of Power Sources, 195 (2010) 939-954.

[8] Megahed S, Scrosati B (1994) Lithium-ion rechargeable batteries. J Power Sources 51:79–104.

[9] Goriparti et al. / Journal of Power Sources 257 (2014) 421-443

[10] Palmieri, Alessandro, et al. "Metal Oxide/Reduced Graphene Oxide Anodes for Lithium-Ion Batteries." *ECS Transactions* 66.9 (2015): 47-55.

[11] Wang, F.M., Yu, M.H., Hsiao, Y.J., Tsai, Y., Hwang, B.J., Wang, Y.Y. and Wan, C.C., 2011. Aging effects to solid electrolyte interface (SEI) membrane formation and the performance analysis of lithium ion batteries. *Int. J. Electrochem. Sci*, *6*, pp.1014-1026.

[12] Z. Chen, I. Belharouak, Y.K. Sun, K. Amine, Adv. Funct. Mater. 23 (2013) 959-969.

[13] Zana, A., Rüdiger, C., Kunze-Liebhäuser, J., Granozzi, G., Reeler, N.E., Vosch, T., Kirkensgaard, J.J. and Arenz, M., 2014. Core-shell TiO 2@ C: towards alternative supports as replacement for high surface area carbon for PEMFC catalysts. *Electrochimica Acta*, *139*, pp.21-28.

[14] Lunell, S.; Stashans, A.; Ojamae, L.; Lindstrom, H.; Hagfeldt, A. J. Am. Chem. Soc. 1997, 119, 7374.

[15] Deng, D.; Kim, M. G.; Lee, J. Y.; Cho, J. Energy EnViron. Sci. 2009, 2, 818.

[16] *J. Am. Chem. Soc., Vol. 119, No. 31, 1997*

[17] Deng, D., Kim, M.G., Lee, J.Y. and Cho, J., 2009. Green energy storage materials: nanostructured TiO 2 and Sn-based anodes for lithium-ion batteries. *Energy & Environmental Science*, *2*(8), pp.818-837.

[18] G. Nuspl, K. Yoshizawa and T. Yamabe, *J. Mater. Chem.*, 1997, **7**, 2529.

[19] Liu, Y. and Yang, Y., 2016. Recent progress of TiO 2-based anodes for Li ion batteries. *Journal of Nanomaterials*, *2016*, p.2.

[20] Wagemaker, M.; Mulder, F. M., *Accounts Chem. Res.* **2012,** *46*, 1206-1215.

[21] Liao, J.Y., Lin, H.P., Chen, H.Y., Kuang, D.B. and Su, C.Y., 2012. High-performance dye-sensitized solar cells based on hierarchical yolk–shell anatase TiO 2 beads. *Journal of Materials Chemistry*, *22*(4), pp.1627-1633.

[22] Das, S. et al. 2010. High lithium storage in micrometre sized mesoporous spherical self-assembly of anatase titania nanospheres and carbon. *Journal of Materials Chemistry*. 20, 8 (2010), 1600–1606.

[23] Kim, M.C., Lee, Y.W., Kim, S.J., Hwang, B.M., Park, H.C., Hwang, E.T., Cao, G. and Park, K.W., 2014. Improved lithium ion behavior properties of TiO 2@ graphitic-like carbon core@ shell nanostructure. *Electrochimica Acta*, *147*, pp.241-249.

[24] Pan, D., Ji, X., An, L. and Lu, Y., 2008. Observation of nucleation and growth of CdS nanocrystals in a two-phase system. *Chemistry of Materials*, *20*(11), pp.3560-3566.

[25] Nguyen, T.D. and Do, T.O., 2009. General two-phase routes to synthesize colloidal metal oxide nanocrystals: simple synthesis and ordered self-assembly structures. *The Journal of Physical Chemistry C*, *113*(26), pp.11204-11214.

[26] Willner, I. and Willner, B., 2001. Molecular and biomolecular optoelectronics. *Pure and Applied Chemistry*, *73*(3), pp.535-542.

[27] Ru-Shi, L. ed., 2012. *Controlled Nanofabrication: Advances and Applications*. CRC Press.

[28] Peng, Y., Chen, Z., Wen, J., Xiao, Q., Weng, D., He, S., Geng, H. and Lu, Y., 2011. Hierarchical manganese oxide/carbon nanocomposites for supercapacitor electrodes. *Nano Research*, *4*(2), pp.216-225.

[29] *D.A.H. Hanaor, C.C. Sorrell, Review of the Anatase to Rutile Phase Transformation, J. Mater. Sci. 46 (2011) 855.*

[30] Shearer, C.J., Slattery, A.D., Stapleton, A.J., Shapter, J.G. and Gibson, C.T., 2016. Accurate thickness measurement of graphene. *Nanotechnology*, *27*(12), p.125704.

[31] Wang, Z. and Lou, X.W.D., 2012. TiO2 nanocages: fast synthesis, interior functionalization and improved lithium storage properties. *Advanced Materials*, *24*(30), pp.4124-4129.

[32] Kruk, M., Jaroniec, M. and Sayari, A., 1997. Application of large pore MCM-41 molecular sieves to improve pore size analysis using nitrogen adsorption measurements. *Langmuir*, *13*(23), pp.6267-6273.

[33] Goriparti, S., Miele, E., De Angelis, F., Di Fabrizio, E., Zaccaria, R.P. and Capiglia, C., 2014. Review on recent progress of nanostructured anode materials for Li-ion batteries. *Journal of Power Sources*, *257*, pp.421-443.

[34] Peng, Y., Le, Z., Wen, M., Zhang, D., Chen, Z., Wu, H.B., Li, H. and Lu, Y., 2017. Mesoporous single-crystal-like TiO 2 mesocages threaded with carbon nanotubes for high-performance electrochemical energy storage. *Nano Energy*, *35*, pp.44-51.

[35] *J. Am. Chem. Soc.*, **2010**, *132* (17), pp 6124–6130.

[36] Zhang, W.F., He, Y.L., Zhang, M.S., Yin, Z. and Chen, Q., 2000. Raman scattering study on anatase TiO2 nanocrystals. *Journal of Physics D: Applied Physics*, *33*(8), p.912.

[37] Liao, Jin-Yun, et al. "High-performance dye-sensitized solar cells based on hierarchical yolk–shell anatase TiO 2 beads." *Journal of Materials Chemistry* 22.4 (2012): 1627-1633.

[38] J. Y. Shin , D. Samuelis , J. Maier , *Adv. Funct. Mater.* **2011** , *21* , 3464 .

[39] Lou, X. W.; Archer, L. A. *Ad*V*. Mater.* **2008**, *20*, 1853.

[40] Das, S.K., Darmakolla, S. and Bhattacharyya, A.J., 2010. High lithium storage in micrometre sized mesoporous spherical self-assembly of anatase titania nanospheres and carbon. *Journal of Materials Chemistry*, *20*(8), pp.1600-1606.

[41] D. Dambournet, I. Belharouak, K. Amine, Tailored Preparation Methods of TiO2 Anatase Rutile, Brookite: Mechanism of Formation and Electrochemical Properties, Chem. Mater. 22 (2010) 1173. *Chem. Mater.*, **2010**, *22* (3), pp 1173–1179.

[42] Cheng, Y., Chen, Z., Wu, H., Zhu, M. and Lu, Y., 2016. Ionic Liquid-Assisted Synthesis of TiO2–Carbon Hybrid Nanostructures for Lithium-Ion Batteries. *Advanced Functional Materials*, *26*(9), pp.1338-1346.

[43] Jang, Jihyun, et al. "A First-Cycle Coulombic Efficiency Higher than 100% Observed for a Li2MO3 (M= Mo or Ru) Electrode." *Angewandte Chemie International Edition* 53.40 (2014): 10654-10657.

[44] Peng, Y., Chen, Z., Wen, J., Xiao, Q., Weng, D., He, S., Geng, H. and Lu, Y., 2011. Hierarchical manganese oxide/carbon nanocomposites for supercapacitor electrodes. *Nano Research*, *4*(2), pp.216-225.

[45] Segall, M. D., et al. "First-principles simulation: ideas, illustrations and the CASTEP code." *Journal of Physics: Condensed Matter* 14.11 (2002): 2717.